Accepted Manuscript

Influence of High Fidelity Structural Models on the Predicted Mass of Aircraft Wing Using Design Optimization

Odeh Dababneha, Timoleon Kipouros

PII: S1270-9638(18)30211-6
DOI: https://doi.org/10.1016/j.ast.2018.05.043
Reference: AESCTE 4596

To appear in: *Aerospace Science and Technology*

Received date: 27 January 2018
Revised date: 17 April 2018
Accepted date: 23 May 2018

Please cite this article in press as: O. Dababneha, T. Kipouros, Influence of High Fidelity Structural Models on the Predicted Mass of Aircraft Wing Using Design Optimization, *Aerosp. Sci. Technol.* (2018), https://doi.org/10.1016/j.ast.2018.05.043

Aerospace Science and Technology, Volume 79, August 2018, Pages 164-173
DOI: 10.1016/j.ast.2018.05.043

Influence of High Fidelity Structural Models on the Predicted Mass of Aircraft Wing Using Design Optimization

Odeh Dababneh[a]*, Timoleon Kipouros[b,c]

[a]*School of Mechanical and Aerospace Engineering, Queen's University Belfast, Belfast, Northern Ireland BT9 5AH, United Kingdom*

[b]*Engineering Design Centre, Department of Engineering University of Cambridge, Cambridge, CB2 1PZ, United Kingdom*

[c]*School of Aerospace, Transport and Manufacturing Cranfield University, Cranfield, MK43 0AL, United Kingdom*

Abstract

This paper explores the necessary and appropriate level of detail that is required to describe the structural geometry of aircraft wings accurately enough to predict the mass of the main load-carrying wing structure to an acceptable level of accuracy. Four different models of increasing structural fidelity are used to describe the wingbox structure of a realistic real-world aircraft wing. The wingbox of the NASA Common Research Model served as a test model for exploring and analyzing the trade-off between the granularity level of the wingbox geometry description under consideration and the computational resources necessary to achieve the required degree of accuracy. The mass of metallic and composite wingbox configurations was calculated via finite element analysis and design optimization techniques. The results provided an insight into the competence of certain wingbox models in predicting the mass of the metallic and composite primary wing structures to an acceptable level of accuracy, and in demonstrating the relative merits of the wingbox structural complexity and the computational time and input efforts for achieving the required level of accuracy.

Keywords: Wing Mass; Primary Wing Structures; High-Fidelity Models; Finite Element; Optimization

Nomenclature

$a_{composite}$	Cross-sectional area of the composite wingbox flanges, mm^2
$a_{metallic}$	Cross-sectional area of the metallic wingbox flanges, mm^2
b	Wing semi-span, m
C	Wing chord length, m
E_{11}	Longitudinal modulus, GPa
E_{12}	Transverse modulus, GPa
E	Elastic modulus, GPa
EI	Bending stiffness
FI	Failure index

*Corresponding author
E-mail address:odeh.da@gmail.com; o.dababneh@qub.ac.uk

G_{12}	In-plane shear modulus, GPa
GJ	Torsional stiffness
$M(\boldsymbol{x})$	Objective function representing the wingbox structural mass
n_{ply}	Number of plies
$t_{metallic}$	Thickness of the metallic wingbox panels, mm
$\delta_{tip(Z)}$	Z-Component of the wingtip displacement
$(\delta)^{+}_{max}$	Maximum vertical displacement in positive direction
$(\delta)^{-}_{max}$	Maximum vertical displacement in negative direction
$\varepsilon_{allowable}$	Allowable strain
$\varepsilon_{principal}$	Principal strain
Θ_{tip}	Angle of twist at the wingtip, deg
$\mu\varepsilon$	Micro strain
ν_{12}	Major Poisson's ratio
$\sigma_{allowable}$	Allowable stress
$\sigma_{von\ Mises}$	von Mises stress
$\sigma_{ultimate}$	Ultimate stress
σ_{axial}	Axial stress

1. Introduction

In a conventional approach to aircraft wing mass estimation at the early stages of the design process, wing mass property design engineers usually follow a particular published methodology, such as one of those proposed by Raymer [1], Roskam [2] or Torenbeek [3]. Taking up as much as 35-50% of the operating empty weight of modern transport aircraft [4], the wing is one of the heaviest structural components of an aircraft. In recent years, aircraft manufacturers and research institutes have been focusing on aircraft concepts that require new wing designs. The NASA Common Research Model (CRM) for a generic transport aircraft model is an example [5,6]. The design of an efficient aircraft wing featuring new technologies has always represented a substantial challenge for aircraft designers, especially when the proposed novel concept challenges the existing knowledge base and the accuracy of normally used empirical methods and statistical data collected from previously constructed aircraft. These methods are generally limited to conventional aircraft designs constructed from light metallic alloys and are unable to assess the relative benefits of novel wing design concepts as well as advanced materials, such as composite materials. In the literature, great efforts have been put into and reported on developing and classifying wing mass prediction methods [7-10]. This is because of the well-defined structural role of the wingbox as a primary load-carrying component and the importance of optimum wing design as a significant subject of the preliminary design phase [11]. The open literature on the subject of wing mass estimation methods and their applications in the aerospace industry has been comprehensively discussed by Dababneh and Kipouros in [12]. In their work, the current state of the art of aircraft wing mass estimation methods has been reviewed. Special attention has been given to classifications of wing mass

estimation methods and to the current challenges and technological difficulties in wing mass estimation methods. According to [12], determining the mass of an aircraft wing, for which the database is insufficient or non-existent or the wing design lies beyond the use of empirical methods, via fully integrated finite element analysis [13-17], and design optimization methods [18,19,20] appears to be a promising approach to consider at the early stages of the design process. This has been made possible over the last 10 years by the increased processing power of computers, the advancements in computer-aided design, the enhancement of multi-dimensional design space visualizations, simultaneous calculation, visual screening and representations of a variety of design analysis and optimization results [21]. With design optimization, one is usually concerned with the chosen form of the structural model and the finite element level of detail in the wingbox that is needed to be considered in order to achieve the required results. Ciampa et al. [22] highlighted the importance of significantly reduced complexity finite element models in the pre-design phase process of aircraft wing structures. In their work, they showed that the wing skin stiffened panels can be represented by stiffness-equivalent panels. This procedure enables a fast search for an optimum mass with low computational resources, but does not provide enough information for the sizing of stiffened panels. In another example, Yang et al. [23], revealed that adequate natural frequency and mode shape results for a complex wing structure can be achieved by using an equivalent wing model, in which each wing segment is modeled as equivalent plate, reducing the wing structural complexity to a simple model and hence the cost of the design task. In the field of structural design optimization concepts for aerospace industry, Ritter [24] showed that while the industry-standard beam-rod representation of aircraft wing is sufficient for linear aeroelastic simulations, a 3D wingbox model, which resembles a real aircraft wing much more realistically, will provide valuable insight into the aeroelastic dynamic behavior of the structure especially when the design optimization process is focused on aeroelastic tailoring [25]. The scope of this study is to investigate and understand the effect of using different wingbox configurations of increasing structural complexity on the mass estimation of the wing primary structure. The goals of the present study are mainly twofold. The first is to identify and select an appropriate model that can predict the mass of the CRM wingbox to an acceptable level of accuracy. It also has to allow the designer to explore and asses the design decisions made, such as the choice of construction material, at an early stage of the design process, thus eliminating any costly changes during the detailed design process, and can serve as well as a baseline model for future complex structural optimization studies. The second is to demonstrate the trade-off between the wingbox structural complexity models under consideration and the user input efforts and computational time needed to achieve sufficiently accurate results for the intended design and analysis purposes.

2. Technical description of the CRM wing

The CRM is a modern single-aisle transport-class aircraft configuration that was generated as an open geometry for collaborative research within the aerodynamics community. It has a wingspan of 58.76 m, a mean aerodynamic chord of 7.0 m, an aspect ratio of 9.0, a taper ratio of 0.275, a leading edge sweep angle of 35°, a break along the trailing edge at 37% of the semi-span (also referred to as the yehudi break), a wing tip chord of 2.73 m, a wing root chord of 13.56 m and a cruise Mach number of 0.85. The

maximum take-off mass (MTOM) is set to 260,000 kg. The maximum cruise speed limit is set to V_C = 193 m/s EAS with a cruise Mach number of M_C = 0.85. The dive speed is set to V_D = 221.7 m/s EAS with a dive Mach number of M_D = 0.92, which results from the equation $M_D = M_C + 0.07$ given in [26]. The cruise altitude is taken as 10,668 m. The planform of the wing and the relevant data are presented in Fig. 2.

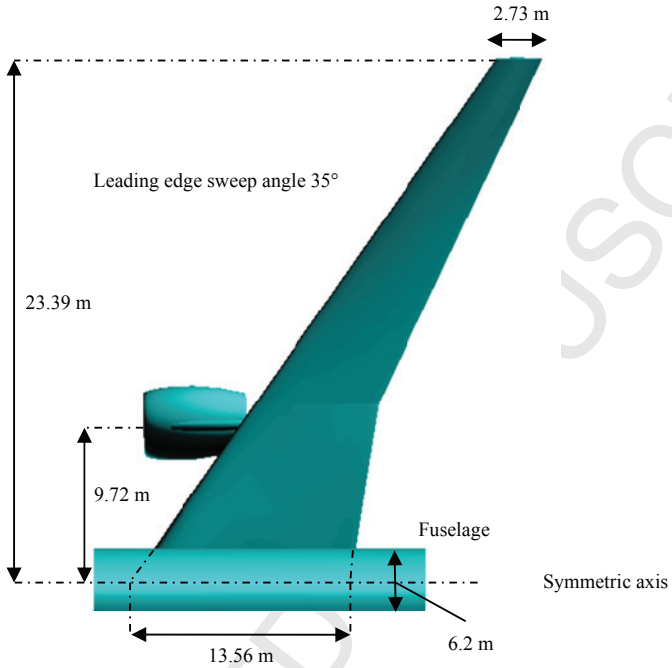

Fig. 2 Planform of the CRM wing

3. Structural and finite element modeling of the CRM wing

The CRM primary wing structure is modeled to meet the minimum design requirements set forth in the Federal Aviation Regulations (FAR) Part 25 [27] and/or the European Aviation Safety Agency (EASA) CS-25 [26]. Traditional two-spar wingbox architecture is used as a baseline design. The external geometry is defined by CRM.65-BTE airfoil sections and the wingbox is derived from the wing surface model by defining the front and rear spar positions at 12% and 71% of the local airfoil chord. The internal layout is defined by the stiffener pitch, rib pitch and orientation based on the values for a typical large transport aircraft wing. Fig. 3 shows the CRM wing surface model and the wingbox derived from it.

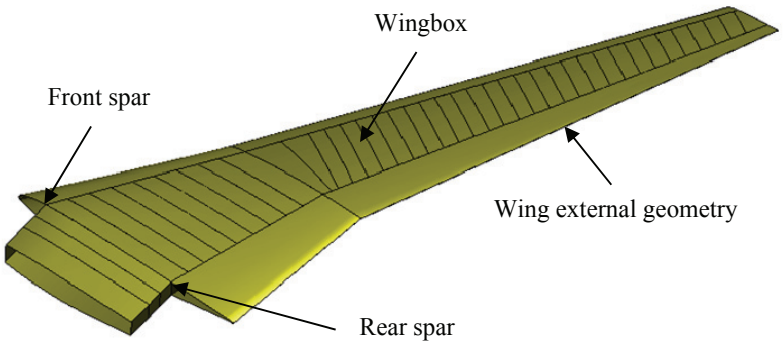

Fig. 3 Surface and wingbox model of the CRM wing

3.1 Description of the considered structural models

The main load carrying wing structure is created using different models of increasing structural fidelity, as shown in Figs. 4-7. The main goal is to identify and select an appropriate model that can predict the mass of the primary wing structure to an acceptable level of accuracy. This done by conducting comparative effectiveness studies that aim to investigate the effects of using different wingbox configurations on the definition of the analysis and optimization models, and therefore on the wingbox mass estimation.

1. Wingbox section model 1

In this model, as shown in Fig. 4, each bay in the wingbox is modeled by four un-stiffened thin-walled panels. These panels represent the upper and lower skins of the wingbox, as well as the front and rear spar webs. The thicknesses of the panels are treated as independent design variables representing the wing torsion box and contributing to bending strength properties.

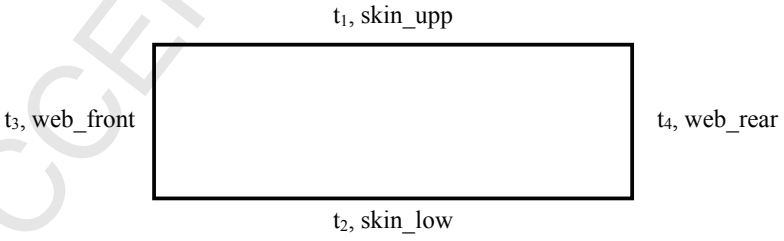

Fig. 4 Wingbox section Model 1 and related design parameters

2. Wingbox section model 2

This model, as shown in Fig. 5, retraces the previous one and considers the rib thickness as a fifth independent design variable. The number of ribs and their spacing is determined from previously acquired knowledge and evidence from other engineering designs. The ribs and their spacing must maintain the aerodynamic shape of the wing and provide enough clearance through the access hole between each rib

section for inspections and maintenance throughout the operational life of the aircraft. A better evaluation and understanding of the wingbox in-plane and out-of-plane stiffness and bending requirements is hoped to be gained using this model.

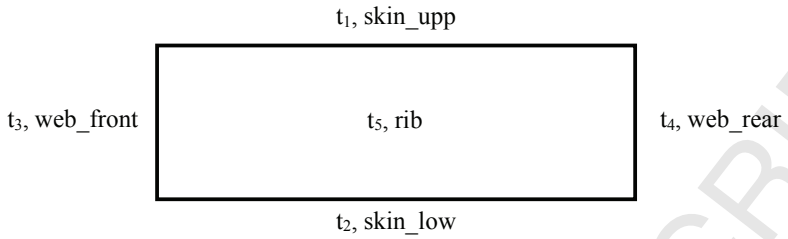

Fig. 5 Wingbox section Model 2 and related design parameters

3. Wingbox section model 3

Four additional independent design variables are added to the third model: upper and lower spar caps are added to the front and rear spars, as illustrated in Fig. 6. The spar caps take most of the loads from the bending moments, and due to the presence of the spar web, one cap experiences a tension force while another undergoes compression. The spar caps' cross-sectional areas are usually large and vary along the wing.

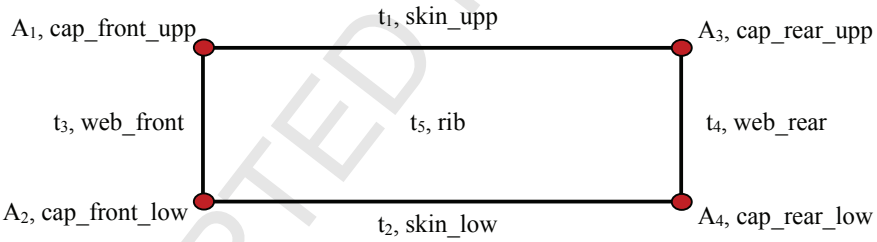

Fig. 6 Wingbox section Model 3 and related design parameters

4. Wingbox section model 4

Stiffeners are added as new independent design variables to the previous model, as shown in Fig. 6. They are used to support the skin between the ribs and to account for the instability of the thin-walled panels. The stiffeners are also used to resist the part of the bending moment which is not resisted by the spar caps and to take some of the tension and compression loads with effective skin areas. The number of stiffeners and the distance between them is determined from previous design experience.

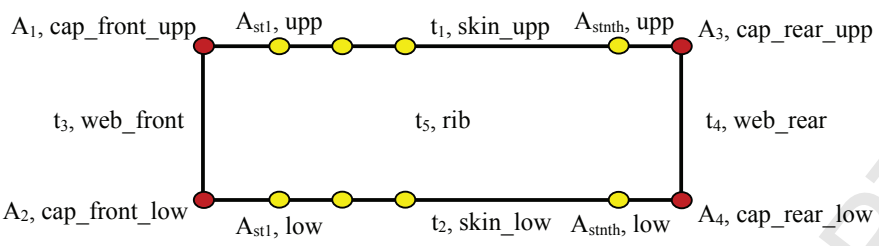

Fig. 7 Wingbox section Model 4 and related design parameters

The wingbox of the CRM aircraft is designed by considering both metallic and composite materials, which have a high strength-to-weight ratio for lightweight structures, high strength and stiffness properties, good fatigue and corrosion resistance. High-strength aluminum 7050-T7451 alloy [28] is used for the design of the upper skins, upper stringers and spar caps of the wingbox, and 2024-T351 alloy [29] is used for the design of the lower skins, lower stringers and the ribs, since it is better suited for structures stressed by cyclic tension loads and therefore prone to fatigue damage. In addition to aluminium alloys, composite materials made up of T300 carbon fibres and N5208 epoxy resin, which is widely used in the aircraft industry, is used as a second material choice for the wingbox structure design [30]. For modeling the wingbox using a composite material, a symmetric and balanced laminate with ply orientation angles of [45/0/-45/90]s was created in order to get an orthotropic material. The aim of this design procedure was to avoid shear extension and membrane bending coupled behaviors.

3.2 Aerodynamic loads calculation of the CRM wing

For the CRM wing, the design loads are obtained from two scenarios, related to flight maneuvers and gust conditions, in accordance with the standard airworthiness certification regulations [26,27]:

1. Symmetric pull-up maneuver load for the maximum positive limit load factor at maximum take-off mass and maximum dive speed, V_D, at sea-level standard atmospheric conditions;
2. Gust loads for the maximum gust load factor at maximum zero fuel mass and maximum cruise speed, V_C, at a critical gust altitude of 6,100 m.

The symmetric pull-up maneuver at the limit load factor (n = 2.5) at maximum take-off mass (260,000 kg) and design dive speed (V_D = 221.7 m/s EAS, M_D = 0.65) at sea-level conditions was found to be the critical one for the design, analysis and sizing optimization of the CRM wingbox and hence the mass estimation. There are currently several theoretical methods available for determining the aerodynamic loading of an aircraft wing. Many of the theoretical solutions have been programmed for digital computation, and separate computer programs have been used to calculate the aerodynamic forces on an aircraft wing in different flow conditions. The choice of the appropriate method depends on the complexity of the aircraft wing, the purpose of the analysis, the computational cost and the level of accuracy required at the design stage. In the current study, the spanwise lift force and pitching moment were calculated using the ESDU 95010 computer program. ESDUpac A9510 utilizes steady lifting-surface theory based on the Multhopp-Richardson solution to calculate the spanwise loading of wings

with camber and twist in subsonic attached flow [31]. Figs. 8 and 9 give the local overall lift and pitching moment coefficients calculated about a local quarter chord.

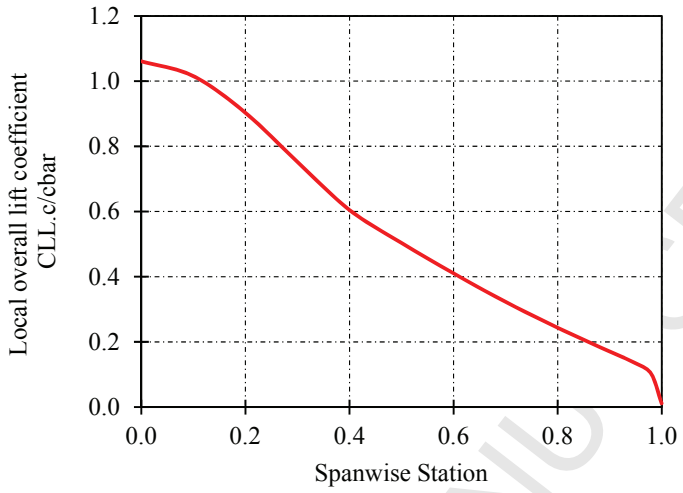

Fig. 8 Spanwise local overall lift coefficient

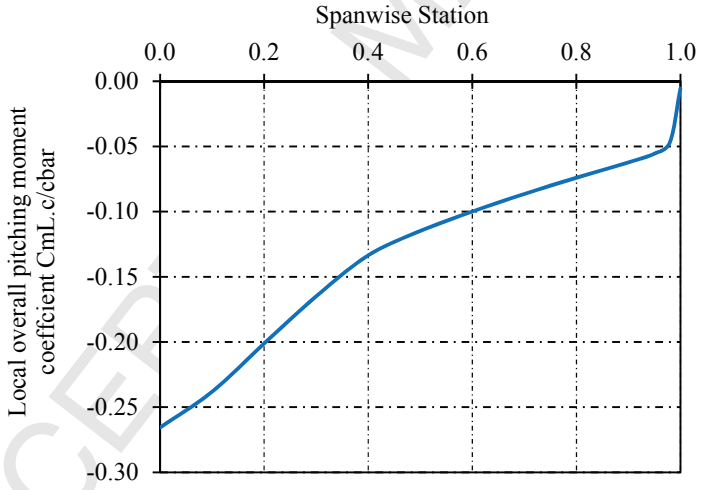

Fig. 9 Spanwise local overall pitching moment coefficient

3.3 Finite element modeling of the CRM wing

In the current study, the thin-walled structures of the CRM wingbox configurations (skins, webs and ribs) were modeled using two-dimensional quadrilateral and triangular shell elements (CQUAD4, CTRAI3) with in-plane membrane and bending stiffness. On the other hand, stringers and spar caps were modeled using one-dimensional rod elements (CROD) with axial stiffness. Finite element models of the CRM wingbox configurations are generated using MSC Patran, based on the physical dimensions and material properties of the structural cross-sectional models as specified in section 3 The wing planform

was modeled for a half-wing section. The structure within the leading and trailing edges was not modeled and the lower skin of the wing has no manholes. Fig. 10 shows the finite element mesh models for the CRM wingbox structures.

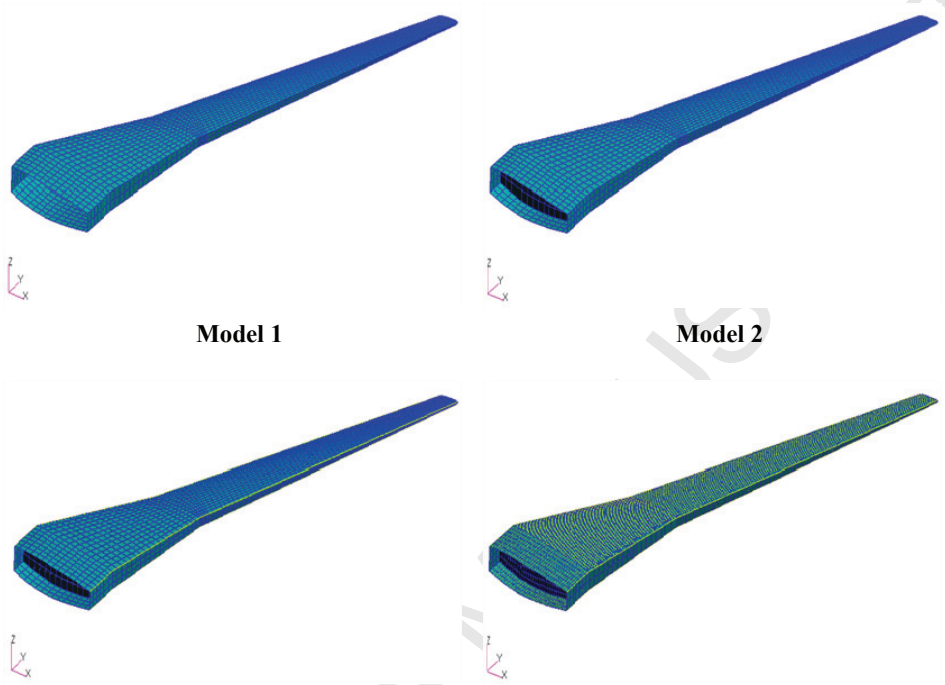

Fig. 11 Finite element mesh models of the CRM wingbox structures-Models 1-4

The aerodynamic loads were discretely distributed along the wing by computing the equivalent lift force and pitching moment components at rib boundary locations at 25% of the local chord length. They were introduced to the wingbox finite element model by means of multipoint constraint (MPC) non-stiffening rigid body elements (RBE3) in the rib's perimeter nodes. Spring elements (CEALS1) combined with RBE2 elements were used to create realistic boundary conditions at the wingbox root at the aircraft centerline. The spring elements were attached to a fixed ground point. The translational and rotational stiffness properties were selected to result in end boundary conditions sufficiently close to the clamped case, due to the lack of available data on wingbox root stiffness values for real aircraft structures in the open literature. The wingbox finite element models have been verified by numerous quality pre-analysis checks, including element free edge, mesh and element quality, boundary conditions, coincident nodes, material and element properties, and element normal. Finite element model checks help to safeguard against fundamental errors, and also guard against the frustration associated with having the solver run for a considerable amount of time, only to abort due to incorrect or missing data.

4. Structural design optimization of the CRM wingbox

Structural optimization methods evolved in the aerospace industry in the late 1950s, when the need to design lightweight structures was critical [32,33,34]. Since then, the aerospace manufacturing industry has shown increasing interest in the application of optimization methods for the optimum design of minimum-weight aircraft structural components [35,36,37]. The survey paper by Venkayya [38] presents an exhaustive review of relevant literature on the structural optimization of aerospace structures. In their work Wang et al. [39] offer numerous and important references on the applications of design optimization approaches to the field of aerospace structure engineering. The CRM wingbox structural optimization that is presented in this work purposely deals with property optimization. Therefore, the locations of the ribs, stiffeners and spars are considered invariable and shape optimization is not performed in this study. The optimization is performed using the commercially available off-the-shelf MSC Nastran gradient-based Sol 200 optimizer [40] which is widely used and recognized by the aerospace industry across the globe. One of the key advantages underlying the selection of gradient-based algorithms is their effectiveness in solving optimization problems where the design space is significantly large, and where the number of design variables is therefore considerably greater than the number of objectives and constraints. Another advantage is their relative computational efficiency due to rapid convergence rates with clear convergence criteria. However, one of the main drawbacks of gradient-based methods is the presence of multiple local optima, resulting in solutions where global optimality cannot be easily guaranteed. In gradient-based methods, global optimality is sought by randomly searching the design space from different starting points. In practice, one normally seeks procedures through which the design search space is explored in a cost-effective manner, aiming for a better optimal solution within an acceptable level of accuracy depending on the size and nature of the optimization problem. For this reason a practical design optimization procedure using gradient-based methods was utilized for the structural sizing for both metallic and composite configuration in order to calculate the mass of the CRM primary wing structure in an effective and efficient way. The reader may wish to refer to the work of Dababneh et al. [41] for more details regarding the practical design optimization framework.

4.1 Structural layout of the CRM wingbox models used for structural optimization

The load-carrying structure of NASA's Common Research Model transport aircraft wing configuration is used for the optimization. Four different wingbox models of increasing structural complexity were created as part of this study. The structural layout of the CRM wingbox models is given in Fig. 11. These models are discretized into components which act as design optimization zones along the span. These areas include the upper and lower skins, front and rear spar webs, ribs, spar caps and stiffeners. Model 1 contains 168 design zones. Model 2 contains 210 design zones. Model 3 contains 378 design zones. Model 4 contains 1,870 design zones. The chordwise design zones are prescribed by the stringer pitch, while in the spanwise direction the design zones are limited by the rib spacing. In the finite element model, each design field consists of a number of finite elements that all comprise the same thicknesses/cross-sectional areas and stiffness properties.

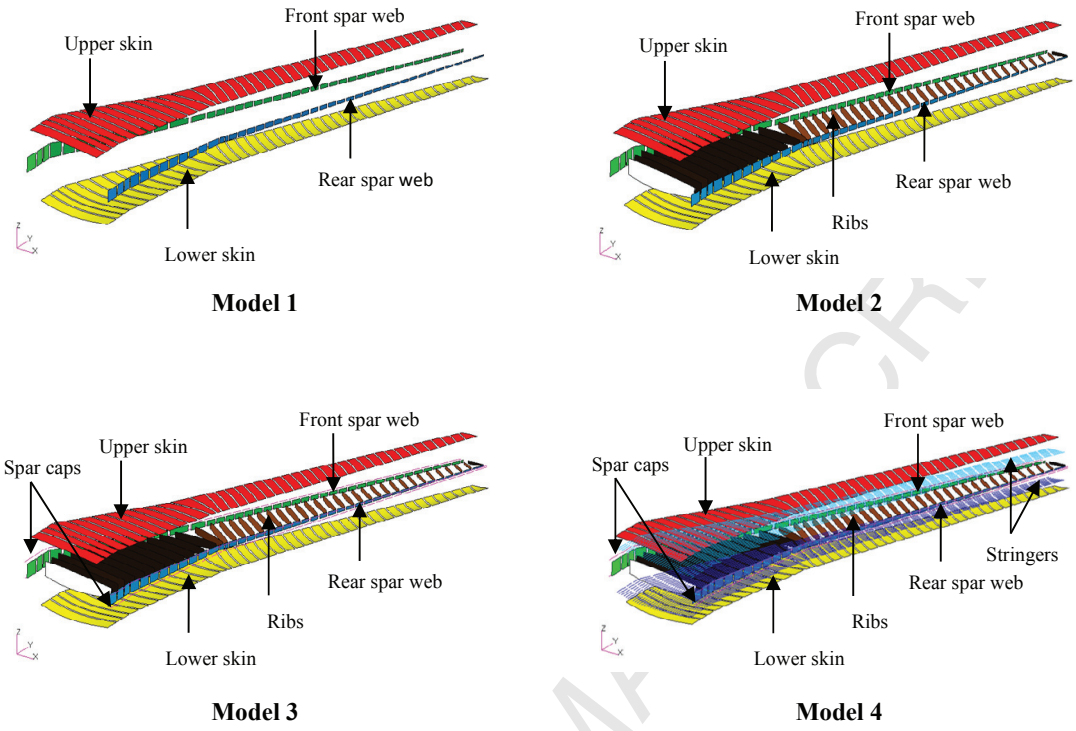

Fig. 11 Design optimization zones of CRM wingbox-Models 1-4

4.2 Formulation of the CRM wingbox optimization problem

During this study, it was decided to formulate this optimization problem in a simple way as possible, in order to stay focused on the main objective and ensure a thorough understanding of the decisions made, including how to solve or eliminate any unusual situations that may arise during the solution process. The masses of the metallic and composite configurations of the CRM wingbox were minimized when subjected to static strength/stiffness constraints on the design variables. The optimization problem mathematically formulated in terms of the objective function, design variables and imposed constraints as follows:

1. Objective function

The objective function is the structural mass of the CRM wingbox. The objective function can be represented by:

$$\text{minimize } M(\boldsymbol{x}), \text{ where } M(\boldsymbol{x}) \text{ is the structural mass of the CRM wingbox} \quad (1)$$

2. Design variables

For the optimization problem, considering the wingbox construction material to be a metallic material, one design variable per design field is defined. The design variables include the thicknesses of the wingbox skins, spar webs and ribs, as well as the cross-sectional areas of the wingbox spar caps and

stiffeners. A minimum gauge thickness of 2 mm and a cross-sectional area of 144 mm^2 are specified for the design variables. The limits on the design variables are defined as follows:

$$2.0 \leq t_{metallic} \tag{2}$$

$$144.0 \leq a_{metallic} \tag{3}$$

On the other hand, considering the wingbox construction material to be a composite material, the corresponding design variables for the wingbox skins, spar webs and ribs are the thicknesses of each ply or lamina in the composite laminate associated with each design field. The cross-sectional areas of the composite spar caps and stiffeners are also treated as individual design variables for each design zone. The minimum ply thickness is taken to be 0.127 mm; while a 3 mm minimum gauge laminate thickness is recommended to maintain an adequate level of laminate damage tolerance. The laminate ply thicknesses are treated as individual design variables and a count is made of the required number of plies in each ply orientation angle. The limits on the number of plies in each ply orientation angle are given as

$$3 \leq n_{ply} \tag{4}$$

Minimum cross-sectional areas of 216 mm^2 for the composite spar caps and stiffeners are specified and the limits on the design variables are defined as

$$216.0 \leq a_{composite} \tag{5}$$

3. Static strength design constraints

For metallic skin panels, spar webs and ribs, the von Mises stress is checked against the material allowable stress as defined in the following equation:

$$\sigma_{\,von\,Mises} \leq \sigma_{\,allowable} \tag{6}$$

For composite skin panels, spar webs and ribs, the Tsai-Wu criterion [42,43,44] is used to predict the strength of the composite laminate in terms of the failure index (FI). For orthotropic plate analysis, under the plane stress state, the Tsai-Wu strength theory predicts that a lamina will undergo failure when the following inequality in satisfied:

$$FI = F_1\sigma_1 + F_2\sigma_2 + F_{11}\sigma_1^2 + 2F_{12}\sigma_1\sigma_2 + F_{22}\sigma_2^2 + F_{66}\sigma_6^2 \geq 1. \tag{7}$$

The coefficients F_1-F_{66}, with the exception of F_{12}, are described in terms of strengths in the principal material directions. F_{12} accounts for the interaction between normal stresses, σ_1 and σ_2.

The principal strains in each ply are also checked against the material allowable strain to ensure the integrity of the plies and failure-free laminates. The allowable strain value of 3500 $\mu\varepsilon$ includes the margins due to fatigue and damage tolerance, assuming that the allowable strains are identical in terms of tension and compression. Thus, the following constraint is placed on the strain value used for sizing the structure:

$$\varepsilon_{\,principal} \leq \varepsilon_{\,allowable} \tag{8}$$

The spar caps and the longitudinal stiffeners are designed to carry axial stress only. Therefore, they are designed according to their stress state against the allowable stress of the material as defined in the following equation:

$$\sigma_{axial} \leq \sigma_{allowable} \tag{9}$$

4. Static stiffness constraints

The flexural stiffness of the wingbox is controlled by limiting the vertical displacement of the wingtip leading edge [45,46]. The wingtip deflection $\delta_{tip(Z)}$ for the CRM wing at a 2.5g pull-up maneuver is assumed to be 15% of the wing semi-span b.

$$\delta_{tip(Z)} \leq 15\% \, . \, b \tag{10}$$

The torsional stiffness, which is necessary to counteract the twisting of the wing under aerodynamic loads and thus prevents flutter, is controlled by constraining the twist angle at the tip chord of the wing. The angular deformation at the wingtip chord is constrained by limiting it to a value of 6° to ensure sufficient torsional stiffness and thus an adequate aeroelastic response [43]. The twist angle constraint is defined using the vertical displacements at the wingtip chord ends. Equation (11) shows that the twist angle at the wingtip should not exceed 6°. $(\delta)^{+}_{max}$ and $(\delta)^{-}_{max}$ are the maximum vertical displacements in positive and negative directions of the z-coordinate, respectively. Here, C is the wing chord length at the required location:

$$\theta_{tip} \leq 6°, \text{where } \theta = \arctan\left(\frac{(\delta)^{+}_{max} - (\delta)^{-}_{max}}{C}\right) \tag{11}$$

4.3 Optimization results of the metallic and composite CRM wingbox models

The CRM wingbox was optimized to meet static strength and stiffness requirements subject to lift force only. In this initial study, no aeroelastic or manufacturing constraints are imposed nor any other types of aerodynamic or inertial forces included, keeping the problem simple and focusing on the effects of using different structural wingbox models for the structural optimization. Moreover, all the design variables for this problem were treated as continuous design variables. The gradient-based optimization algorithm, DOT, was used for the design sizing of the CRM metallic and composite wingbox models. During this initial stage, it was decided to formulate this optimization study in a simple way as possible, in order to stay focused on the main objective and ensure a thorough understanding of the decisions made, including how to solve or eliminate any unusual situations that may arise during the solution process. In the optimization process, the design variables change continuously within a range between a lower limit and an unbounded upper limit. Therefore, the thicknesses and cross-sectional areas of the wingbox model structural components are allowed to vary until all the design requirements are met. During the optimization, convergence is aimed for by using different starting values for the design variables, and the effects of these starting values on the final optimization are investigated. The sets of initial values for the design variables, the thin panel thicknesses, the number of plies in each ply orientation and the flange

cross-sectional areas, for both the metallic and composite CRM wingbox optimization models, are specified as follows:

$$t_{metallic} = \{2, 4, 6, 10, 13\} \text{ mm}, \tag{12}$$

$$n_{ply} = \{3, 4, 8, 11, 15\}, \tag{13}$$

$$a_{metallic} = \{144, 215, 420, 643, 858\} \text{ mm}^2, \tag{14}$$

$$a_{composite} = \{218, 258, 358, 585, 858\} \text{ mm}^2. \tag{15}$$

Tables 1 and 2 show the optimized masses of the metallic and composite CRM wingbox models, respectively, using the sets of initial values for the design variables. Based on the results, it can be seen that by using different initial guesses for the design variables, various local optimum designs can be obtained from the gradient-based optimization solution. In all the solutions, convergence is achieved and the bold values in the tables denote the local minimum solutions obtained for each CRM wingbox model.

Table 1 Optimized masses of metallic CRM wingbox models (kg)

Design variables and initial values				
t_1|a_1	t_2|a_2	t_3|a_3	t_4|a_4	t_5|a_5
Wingbox Model 1				
17,990	18,587	18,641	18,531	17,999
Wingbox Model 2				
12,167	12,271	12,166	**12,149**	12,157
Wingbox Model 3				
12,245	12,129	12,167	12,276	**12,116**
Wingbox Model 4				
12,276	**12,272**	12,325	12,445	12,401

Table 2 Optimized masses of composite CRM wingbox models (kg)

Design variables and initial values				
$\boldsymbol{n_{ply1}}$|a_1	n_{ply2}|a_2	n_{ply3}|a_3	n_{ply4}|a_4	n_{ply5}|a_5
Wingbox Model 1				
12,862	13,468	13,449	13,461	13,514
Wingbox Model 2				
8,535	9,070	9,355	**8,321**	8,587
Wingbox Model 3				
8,373	8,269	9,093	9,058	**7,891**
Wingbox Model 4				
8,917	7,940	**7,192**	8,367	7,366

The optimized masses of the second, third and fourth wingbox models; turned out to be lower than those obtained by the use of the first wingbox model. Therefore, it can be seen that, in the context of using high-fidelity structural models to describe and represent the CRM wingbox design, these models attempt to improve the optimized masses of the wingbox. This representation of the CRM wingbox increases the number of structural elements describing the wingbox from one model to the next. Thus, the number of design variables increases and the design space becomes larger. The possible design alternatives within the design domain thus increase, thereby increasing the chances of arriving at a better local optimum solution and mass estimate.

The optimized masses of the composite wingbox models indicate that the results are more sensitive to their initial starting values for the design variables than the results of the metallic wingbox models. In this case, there is a greater difference in the optimized masses between the composite wingbox models than for the metallic wingbox models. This behavior can be explained by the different mechanical properties of the composite laminate, which are more complex than those of the metallic material. The global laminate properties are dependent on the fiber orientation angles, the number of layers and their thicknesses, and the stacking sequence. For an orthotropic material, at least two elastic constants are needed to describe the stress-strain behavior in the material. Therefore, the stiffness of an orthotropic plate must be described by two values, one along the longitudinal direction of the fibers, commonly referred to as E_L, and one transverse to the direction of the fibers, usually denoted by E_T. Using classical lamination theory [42,43,44], the bending stiffness matrix of the symmetric laminate $[\boldsymbol{D}]$ can be written as

$$[\boldsymbol{D}] = \frac{2}{3}\sum_{k=1}^{n_{ply}} [\bar{\boldsymbol{Q}}]_K \, (Z_k^3 - Z_{k+1}^3), \tag{16}$$

where $[\bar{\boldsymbol{Q}}]_K$ is the transformed reduced stiffness matrix of the kth layer, $(Z_k - Z_{k+1})$ is the ply thickness and n_{ply} is the number of plies. The transformed reduced stiffness matrix can be defined in terms of the ply angle ϕ and the elastic constants E_{11}, E_{22}, ν_{12} and G_{12} of the orthotropic layer. The mathematical derivation of $[\bar{\boldsymbol{Q}}]_K$ can be found in [42,43]. On the other hand, the bending stiffness k_b of beam-like metallic structures under an applied force F [48,49], as shown in Fig. 12, can be defined as

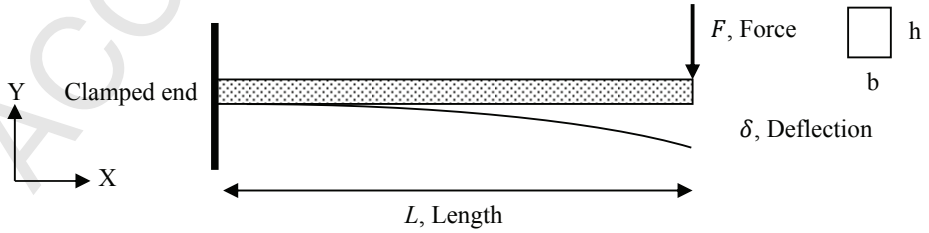

Fig. 12 Deflection of cantilevered beam

$$k_b = \frac{F}{\delta} = \frac{3EI_{xx}}{L^3}\text{, where } I_{xx} = \frac{1}{12}\text{bh}^3, E \text{ is Young's Modulus.} \tag{17}$$

Mathematically, the area moment of inertia I_{xx} appears in the numerator of the stiffness equation, Eqn. (17), therefore the larger the area moment of the inertia, the less the structure deflects and thus the greater the stiffness. According to Eqns. (16) and (17), the derivation of the composite laminate bending stiffness with respect to the layer thickness is a bit more complex than for the metallic isotropic material, where the stiffness is described by one constant value; the modulus E of the material regardless of the direction of load. An infinitesimal change in the composite layer thickness has an influence on its own stiffness and on the stiffness of all the layers above. We can therefore create an equivalent design with the same bending stiffness by changing the thicknesses of the composite layers while preserving the original ply orientation of each layer and the same total thickness of the laminate. The existence of multiple laminate equivalent designs has important implications for the optimization process, in that it results in multiple optima and will always have a major influence on the objective function value.

The accuracy of the four proposed wingbox models in predicting the mass of the primary wing structure is analyzed using the estimated optimum mass of the fourth wingbox model m_4 as a reference value. Table 3 shows the errors of the wingbox masses predicted using the four different models of increasing structural complexity. The error has been calculated as

Table 3 Errors of the wingbox mass estimation

Wingbox Model	Metallic [%]	Composite [%]
Model 1	31.78	44.08
Model 2	-1.01	13.57
Model 3	-1.29	8.86
Model 4	0.00	0.00

From Table 3, it is observed that the first wingbox model over predicts the primary wing structure mass for the CRM aircraft in comparison with the other models. A possible cause for this larger deviation of Model 1 can be explained by the lack of internal chordwise oriented wing structural elements, meaning that the wing skins have to carry an additional part of the lift load that is usually transferred to the wing main spar by the ribs. Furthermore, the first wingbox model is a hollow beam and is less efficient than the rest of the models, which contain ribs with hybrid orientation, in torsional stiffness. As a consequence, the wingbox skin thicknesses are increased, resulting in an increase in the mass of the wingbox. From the results summarized in Table 3, it can be seen that the second and third metallic wingbox models show good accuracy with errors of -1.01 and -1.29%, respectively, for the mass estimation of the CRM wingbox. For the composite wingbox models, this is not the case. The second and third composite wingbox models over predict the primary wing structure mass for the CRM aircraft with errors of 13.57 and 8.86%, respectively.

The total wall-clock time for each optimization run until convergence occurs and an optimum solution has been found is also compared, and the summary of the computational time is shown in Table 4. In this study, computations were carried out on a laptop computer with a 2.60 GHz Intel i5 CPU and 8GB RAM. From the results given in Table 4, it can be seen that the computational times for the optimized composite

models are very long compared to the optimized metallic models, as the design space for the composite models is relatively complex with a large number of design variables and constraints. Furthermore, it is also observed that the optimization run time was significantly increased for the fourth wingbox mass estimation model for both the metallic and composite CRM wingbox configurations. Despite the long run time, the fourth wingbox model is shown to have improved the accuracy of the objective function value, particularly for the CRM composite wingbox model, as explained in the foregoing discussion of the results presented in Table 3.

Table 4 Total wall-clock time (seconds)

Wingbox Model	Metallic [s]	Composite [s]
Model 1	55.5	562.6
Model 2	55.9	497.1
Model 3	63.9	662.9
Model 4	742.4	5,303.4

The values of the CRM wingbox mass obtained in the current study are compared with the estimated mass values according to the open scientific literature. It should be noted that no mass values were reported for the composite CRM wingbox in the literature. Generally, the wingbox mass value of the metallic CRM wing calculated in the current study is in good agreement with the value estimated (12,263kg) by Kenway et al. [50]. On the other hand, the CRM wingbox mass (11,494 kg) calculated by Klimmek [51] is lower than the mass reported in the current study. Possible sources for discrepancies can be traced to the location of the spars and the number of ribs, as well as their spacing and location, which have a direct effect on the wingbox mass. Flight conditions for the calculation of sizing loads and/or aerodynamic loads, the definition and number of design variables and constraints in the scenario of using optimization techniques.

5. Concluding remarks

Based on the results presented in Tables 1 and 2 in this study, the following points could be concluded:

- In a scenario where high-fidelity structural models are used to describe and represent the CRM wingbox model, these models do indeed attempt to improve the optimized masses of the wingbox. This representation of the CRM wingbox increases the number of structural elements describing the wingbox from one model to the next. Thus, the number of design variables increases, and the design space enlarges. The possible design alternatives within the design domain then increase, which in turn increases the chances of arriving at a better local optimum solution and mass estimate.
- The mass of the metallic CRM wing box can be estimated with an acceptable level of accuracy and reduced computational time with high degree of confidence by using the second wingbox model of structural fidelity, as long as the gradient-based designs are also optimized using a sufficient

number of different starting values for the design variables, as practiced in the design and optimization phase of this study (See Table 1).

- In the scenario where composite materials are used as the primary construction material for the design of the CRM wingbox, it is observed that by increasing the structural fidelity of the wingbox model, as observed in the second and third wingbox models, the discrepancy in the mass estimate becomes smaller but still significant. Therefore, it is strongly recommended that the fourth wingbox model be used as the baseline model for the preliminary estimate of the composite CRM wingbox mass, requiring higher computational time in order to achieve the required accuracy level.
- The optimized masses of the composite wingbox models indicate that the results are more sensitive to the initial starting values of the design variables than to the results of the metallic wingbox models (See Table 1 and 2). In this case, the change in the optimized masses of the composite wingbox models is larger than the change for the metallic wingbox. This behavior can be explained by the different mechanical properties of the composite laminate, which are more complex than those of metallic structures. The computational times for the optimized composite models are long and the design space is relatively complex, with a large number of design variables and constraints compared to the optimized metallic models.

6. Future work

In the view of the above, and for a more detailed insight into the CRM wingbox mass estimation, further studies that will account for the effects of considering aeroelasticity, buckling, fatigue and damage tolerance, manufacturing requirements, and inertial forces will be considered using multidisciplinary design optimization technique. This will aim to achieve a better understanding of the actual wingbox structural material distributions in terms of thickness and orientation, and finally to assess the structural behavior of the wing, including global displacement and local stresses. This will be a rather appropriate view compared to that from an industrial design perspective.

References

[1] Raymer, D. P. (2006). *Aircraft Design: A Conceptual Approach* (4th ed.). Washington, USA: AIAA Education Series.

[2] Roskam, J. (1989). *Airplane Design: Part III - Layout Design of Cockpit, Fuselage, Wing and Empennage: Cutaways and Inboard Profiles.* Kansas: Roskam Aviation and Engineering Corporation.

[3] Torenbeek, E. (1982). *Synthesis of Subsonic Airplane Design.* Amsterdam: Delft University Press.

[4] Ediger, K., Zeumer, C., & Dugas, M. (2004). *FAME-liA 4.00 F3 - Validation Document.* Technical Report, Airbus Deutschland GmbH.

[5] Klimmek, T. (2014). Parametric Set-Up of a Structural Model for FERMAT Configuration for Aeroelastic and Loads Analysis. *ASDJournal, 3,* (2), 31-49.

[6] Jutte, C. V., Stanford, B. K., & Wieseman, C. D. (2015). *Internal Structural Design of the Common Research Model Wing Box for Aeroelastic Tailoring.* Hampton, Virginia: NASA.

[7] Murphy, N. (1987). *Analytical Wing Weight Prediction/Estimation Using Computer Based Design Techniques.* PhD Thesis, Cranfield Institute of Technology.

[8] Ardema, M., Chambers, M., Patron, A., Hahn, A., Miura, H., & Moore, M. (1996). *Analytical Fuselage and Wing Weight Estimation of Transport Aircraft.* NASA.

[9] Kundu, A. (2010). *Aircraft Design.* Cambridge: Cambridge University Press.

[10] Elham, A. (2013). *Weight Indexing for Multidisciplinary Design Optimization of Lifting Surfaces.* PhD Thesis, Delft University of Technology.

[11] Howe, D. (2000). *Aircraft Conceptual Design Synthesis.* London: Professional Engineering Publishing Limited London and Bury St Edmunds.

[12] Dababneh, O and Kipouros, T (2018). A review of aircraft wing mass estimation methods. *Aerospace Science and Technology*, *72*, 256-266.

[13] Droegkamp, M. (1992). Finite Element Model Weight Estimation. SAWE Paper No. 2089, *51st Annual Conference.* Hartford, Connnecticut: Society of Allied Weight Engineers, Inc.

[14] Zaidel, S. J. (1992). A-12 Structural Target Weight Distribution Using the Finite Element Model (FEM). SAWE Paper No. 2110, *51st Annual Conference.* Hartford, Connnecticut: Society of Allied Weight Engineers, Inc.

[15] Mitchell, P. M. (1993). Advanced Finite Element Weight Estimation Process on the High Speed Civil Transport. SAWE Paper No. 2169, *52nd Annual Conference.* Biloxi, Mississippi: Society of Allied Weight Engineers, Inc.

[16] Wenzel, J., Sinapius, U., & Gabbert, U. (2012). Primary Structure Mass Estimation in Early Phases of Aircraft Development using the Finite Element Method. *CEAS Aeronautical Journal, 3* (1), 35-44.

[17] Dababneh, O., & Kayran, A. (2014). Design, analysis and optimization of thin walled semi-monocoque wing structures using different structural idealization in the preliminary design phase. *International Journal of Structural Integrity*, *5* (3), 214-226.

[18] Bindolino, G., Ghiringhelli, G., Ricci, S., & Terraneo, M. (2010). Multilevel Structural Optimization for Preliminary Wing-Box Weight. *Journal of Aircraft, 47, No. 2*, 475-489.

[19] Hurlimann, F., Kelm, R., Dugas, M., Oltmann, K., & Kress, G. (2010). Mass estimation of transport aircraft wingbox structures with a CAD/CAE-based multidisciplinary process. *Aerospace Science and Technology, 15* (4), 323-333.

[20] Dorbath, F., Nagel, B., & Gollnick, V. (2012). A Knowledge Based Approach for Extended Physics-Based Wing Mass Estimation in early Design Stages. *28th Congress of the International Council of the Aeronautical Sciences. 6.* Brisbane: ICAS.

[21] Holden, C. M., & Keane, A. J. (2004). Visualization Methodologies in Aircraft Design. AIAA-2004-4449. *10th AIAA/ISSMO Multidisciplinary Analysis and Optimization Conference.* Albany, New York.

[22] Ciampa, P. M., Nagel, B., & Tooren, M. (2010). Global Local Structural Optimization of Transportation Aircraft Wings. AIAA 2010-3098. *51st AIAA/ASME/ASCE/AHS/ASC Structures, Structural Dynamics, and Materials Conference.* Orlando, Florida: AIAA.

[23] Yang, Y., Wu, Z., & Yang, C. (2012). Equivalent Plate Modeling for Complex Wing Configurations. *Procedia Engineering, 31,* 409-415.

[24] Ritter, M., & Cesnik, C. (2016). Large Deformation Modeling of a Beam Type Structure and a 3D Wingbox using an Enhanced Modal Approach. AIAA 2016-1708. *57th AIAA/ASME/ASCE/AHS/ASC Structures, Structural Dynamics, and Materials Conference.* San Diego, California: AIAA.

[25] Werter, N., & Breuker, R. (2015). Aeroelastic tailoring and structural optimization using an advanced dynamic aeroelastic framework. *IFASD 2015: 16th International Forum on Aeroelasticity and Structural Dynamics Conference*. Saint Petersburg, Russia.

[26] EASA. (2015). *Certification Specifications and Acceptable Means of Compleance for Large Aeroplanes CS-25, Amendment 16.* Retrieved March 28, 2015, from http://easa.europa.eu/system/files/dfu/CS-25 20Amdendment 16.pdf

[27] FAA. *FAR 25, Airworthiness Standards: Transport Category Airplanes* (*Title 14 CFR Part 25*). Retrieved January 15, 2014, from http://flightsimaviation.com/data/FARS/part_25.html

[28] ASM. (1978). *ASM Aerospace Specification Metals, Aluminum 7050-T7451*. Retrieved June 12, 2014, from http://asm.matweb.com/search/SpecificMaterial.asp?bassnum=MA7050T745

[29] ASM. (1978). *ASM Aerospace Specification Metals, Aluminum 2024-T3*. Retrieved June 12, 2014, from http://asm.matweb.com/search/SpecificMaterial.asp?bassnum=%20MA2024T3

[30] Soni, S. R. (1980). *Elastic Properties of T300/5208 Bidirectional Symmetric Laminates - Technical Report Afwal-Tr-80-4111*. Ohio 45433: Materials Laboratory - Air Force Wright Aeronautical Laboratories - Air Force Systems Command.

[31] ESDU. (1999). *Computer program for estimation of spanwise loading of wings with camber and twist in subsonic attached flow. Lifting-surface theory*. Retrieved March 12, 2014, from https://www.esdu.com/cgi-bin/ps.pl?sess=cranfield5_1160220142018cql&t=doc&p=esdu_95010c

[32] Brennan, J. (1999). Integrating Optimization into the Design Process. *Proceedings of the Altair HyperWorks Technology Showcase.* London.

[33] Cervellera, P. (2004). Optimization Driven Design Process: Practical Experience on Structural Components. *Proceedings of the 14th Convegno Nazionae ADM.* Bari.

[34] Gartmeier, O., & Dunne, W. L. (1999). Structural Optimization in Vehicle Design Development. *MSC. Worldwide Automotive Conference.*

[35] Krog, L., Tucker, A., & Rollema, G. (2002). Application of Topology, Sizing and Shape Optimization Methods to Optimal Design of Aircraft Components. *3rd Altair UK HyperWorks Users Conference.*

[36] Krog, L., Tucker, A., Kempt, M., & Boyd, R. (2004). Topology Optimization of Aircraft Wing Box Ribs, AIAA-2004-4481. *Proc. 10th AIAA/ISSMO Symposium on Multidisciplinary Analysis and Optimization.* Albany, NY.

[37] Schumacher, G., Stettner, M., Zotemantel, R., O'Leary, O., & Wagner, M. (2004). Optimization Assisted Strcutural Design of New Military Transport Aircraft, AIAA-2004-4641. *Proc. 10th AIAA MAO Conference.* Albany, NY.

[38] Venkayya, V. B. (1971). Design of Optimum Strcutures. *Computers and Structures* (No.1), 265-309.

[39] Wang, Z., Huang, W. & Yan, L. (2014). Multidisciplinary design optimization approach and its application to aerospace engineering. *Chinese Science Bulletin*, 59, (36), 5338-5353

[40] MSC Nastran (2012). *Design Sensitivity and Optimization User's Guide*. Santa Ana, CA: MSC.Software Corporation.

[41] Dababneh O, Kipouros T & Whidborne JF (2018). Application of an efficient gradient-based optimization strategy for aircraft wing structures, *Aerospace*, *5*, (1), 1-27.

[42] Jones, R. M. (1999). *Mechanics of Composite Materials* (2nd ed.). Taylor & Francis.

[43] Tsai, S. W., & Hahn, H. T. (1980). *Introduction to Composite Materials.* Technomic Publishing Co.

[44] Kassapoglou, C. (2013). *Review of Laminate Strength and Failure Criteria, in Design and Analysis of Composite Structures: With Applications to Aerospace Structures.* Oxford: John Wiley & Sons Ltd.

[45] Starnes Jr, J. R., & Haftka, R. T. (1979). Preliminary Design of Composite Wings for Buckling, Stress and Displacement Constraints. *Journal of Aircraft, 16* (8), 564-570.

[46] Oliver, M., climent, H., & Rosich, F. (1999). Non Linear Effects of Applied Loads and Large Deformations on Aircraft Normal Modes. *RTO AVT Specialists' Meeting on Strucrural Aspects of Flexible Aircraft Control.* Ottawa.

[47] Liu, Q., Mulani, S., & Kapani, R. K. (2014). Global/Local Multidisciplinary Design Optimization of Subsonic Wing, AIAA 2014-0471. *10th AIAA Multidisciplinary Design Optimization Conference - AIAA SciTech.* National Harbor, Maryland: AIAA, Inc.

[48] Niu, M. C. (1999). *Airframe Stress Analysis and Sizing.* Conmilit Pres Ltd.

[49] Beer, F., Johnston, J. E., DeWolf, J., & Mazurek, D. (2014). *Mechanics of Materials* (7th ed.). McGraw-Hill Education.

[50] Kenway, G. K., Martins, J. R., & Kennedy, G. J. (2014). Aerostructural optimization of the Common Research Model configuration, AIAA 2014-3274. *15th AIAA/ISSMO Multidisciplinary Analysis and Optimization Conference.* Atlanta, GA: AIAA Aviation.

[51] Klimmek, T. (2014). Parametric Set-Up of a Structural Model for FERMAT Configuration for Aeroelastic and Loads Analysis. *ASDJournal, 3, (2), 31-49.*